RESEARCH ARTICLE | FEBRUARY 02 2017

Analysis and application of neuronal network controllability and observability

Fei Su; Jiang Wang; Huiyan Li; Bin Deng ; Haitao Yu; Chen Liu

Chaos 27, 023103 (2017)
https://doi.org/10.1063/1.4975124

Analysis and application of neuronal network controllability and observability

Fei Su,[1] Jiang Wang,[1] Huiyan Li,[2] Bin Deng,[1] Haitao Yu,[1,a)] and Chen Liu[1]
[1]*School of Electrical Engineering and Automation, Tianjin University, Tianjin 300072, China*
[2]*School of Automation and Electrical Engineering, Tianjin University of Technology and Education, Tianjin 300222, China*

(Received 13 November 2016; accepted 18 January 2017; published online 2 February 2017)

Controllability and observability analyses are important prerequisite for designing suitable neural control strategy, which can help lower the efforts required to control and observe the system dynamics. First, 3-neuron motifs including the excitatory motif, the inhibitory motif, and the mixed motif are constructed to investigate the effects of single neuron and synaptic dynamics on network controllability (observability). Simulation results demonstrate that for networks with the same topological structure, the controllability (observability) of the node always changes if the properties of neurons and synaptic coupling strengths vary. Besides, the inhibitory networks are more controllable (observable) than the excitatory networks when the coupling strengths are the same. Then, the numerically determined controllability results of 3-neuron excitatory motifs are generalized to the desynchronization control of the modular motif network. The control energy and neuronal synchrony measure indexes are used to quantify the controllability of each node in the modular network. The best driver node obtained in this way is the same as the deduced one from motif analysis. *Published by AIP Publishing.* [http://dx.doi.org/10.1063/1.4975124]

Currently, how to optimally control the neural network dynamics towards a desired state is a research focus. The study on network controllability and observability can help design a more suitable control framework. However the complex characteristics of the neural network, including single neuron dynamics, synaptic type, and network topological structure make this process quite challenging. Previous studies mainly focused on the relationship between network topological structure and the controllability (observability) of the node. To make progress, here we first explore the effects of node and synaptic dynamics on its controllability (observability) based on 3-neuron motif networks. After that, we intend to generalize analysis results of 3-neuron motif networks to a larger network. The desynchronization control of a modular motif network is carried out. The node with the minimum control energy needed to desynchronize the network dynamics is defined as the best driver node. Interestingly, the best driver node obtained from this way is the same as the one generalized from motif analysis.

I. INTRODUCTION

Neural control underlies an expanding range of application, including the development of neuroprosthetics,[1] cellular electrophysiology,[2,3] and the rehabilitation of neurological diseases.[4,5] Generally speaking, neural control means modulating the neural system towards a desired state by stimulating certain neural tissues. In spite of numerous efforts done by researchers, the optimal control method is yet to be discovered, which is in part due to the complex interplay of neural elements and the large number of unobservable variables in the system., thus raising the question of which target best controls (observes) the overall network behavior. There are two key concepts here from the viewpoint of control theory: controllability and observability.[6,7] A high controllability is correlated with less effort and energy consumption needed to control the system; meanwhile, a high observability corresponds to the high estimation accuracy of hidden states.[8]

As for the research on controllability and observability, significant efforts went into the field of complex networks. The main contribution was made by Liu *et al.* who hold that the dynamic properties of complex systems could be learned from their topological structures.[9] Yuan *et al.* developed the exact controllability framework to measure the controllability of undirected networks, where the minimum number of driver nodes was determined by the maximum geometric multiplicity of the eigenvalue of the system coupling matrix.[10] Follow-up studies systematically explored the controllability of complex networks with arbitrary topological structure, different link weights, and links with or without self-loops based on these two seminal studies.[11–19] As a dual concept of controllability, the relationship between the well-studied network topological structure and observability was carried out in a similar way.[20] All these studies focused mainly on the linear system. Because the authors deemed that the relationship between network topological structure and controllability (observability) of the linear system was a prerequisite of nonlinear problem. Besides, they pointed out that fully exploiting the nonlinear effects was the subject of future research.

The electrophysiology activity of neural networks results from the interplay among the intrinsic properties of

a)Author to whom correspondence should be addressed. Electronic mail: htyu@tju.edu.cn. Tel./Fax: 86-022-27402293.

individual neurons, the type of the synapses, as well as the network topological structure,[21–27] each element plays an important role in shaping the system behavior. What is more, the high nonlinearities of the neural system make it inappropriate to directly use the conclusions of above linear topological structure analysis. Tremendous job has been done in nonlinear controllability and observability. The linearized system near the equilibrium was studied to measure the controllability of the nonlinear system;[28,29] however, the original nonlinear system might be controllable even if the linearized system was not controllable. The method of differential geometry was applied to accurately quantify the controllability (observability) of the nonlinear system, which tied the controllability (observability) to the Lie bracket (derivative). Using the Rossler system, Letellier *et al.* proved that it could be easier to reconstruct the original system dynamics from the variable with high observability.[30] Whalen *et al.* extended the differential geometry method to nonlinear neuronal network motifs with explicit symmetries; the controllability (observability) of nodes was explored as a function of connection topology, measurement nodes, and connection strength, where three nodes were identical.[7] However, they pointed out that the topologically symmetric systems with identical components were extreme cases.

Recent theoretical advances in neural system control demonstrate the role of single neuron and synaptic dynamics in shaping the temporal features of network dynamics.[31–36] Therefore, it is reasonable to infer that the node and synaptic properties do affect the controllability (observability) of the network. But how do they shape the network controllability (observability) was not yet investigated. In general, neurons can be divided into excitatory and inhibitory ones.[37–39] Usually, the topology of neuronal networks is very complex, and a network may include both excitatory and inhibitory neurons. So the controllability (observability) analysis becomes rather challenging, thus motivating recourse to simplifying principles. *Motifs*—small building blocks of large complex networks—represent such a principle.[40–43] "Network motifs" refer to the significant recurring nontrivial patterns of interconnections appeared in large-scale networks, as depicted in Fig. 1; there are thirteen different motifs of size three. Recent studies based on motifs have revealed meaningful mechanisms in resonance[44] and synchronization.[45,46] What is more, model-based approaches to study the neuronal networks usually use highly nonlinear ordinary differential equations to describe the neuronal dynamics,[47] while the symbolic computation of differential geometry is computationally limited to small systems.[48]

On account of the above analyses, this paper intends to prove that the ability to control (observe) a system from particular nodes may depend critically on the dynamics of the nodes and synapses. Such dependence is quantified by a controllability (observability) index, which is obtained through the differential geometry operation.[49] The 3-neuron network motifs with each node modeled as an excitatory or inhibitory neuron are constructed to carry out controllability (observability) analysis. Since the ultimate goal of controllability (observability) analysis is to find a better way to control (observe) the system dynamics, the best driver node calculated through 3-neuron motifs is generalized to the desynchronization control of a modular motif network, which is proved to consume less energy than other nodes.

This paper is organized as follows: In Sec. II, we specify the model of the individual neuron, the synapse as well as the motifs setup, and introduce the index of nonlinear controllability (observability). Controllability (observability) analysis results of motifs are presented in Sec. III. In Sec. IV, we design a closed-loop control framework to realize the desynchronization control of the modular motif network. Finally, conclusions are given in Sec. V.

II. MODEL AND METHOD

A. Network setup

As the main focus of this study is the property of each node and synapse not the network topology, motifs with isolated nodes are not considered here. As for controllability, isolated node means no directed paths reaching the node from the controlled node (e.g., node 1 and 3 in M1). As for observability, isolated node cannot reach the measured node (e.g., node 2 in M1). Therefore, the 3-neuron motifs considered in this paper are M7, M10, M12, and M13. We use "E" and "I" to denote the excitatory and inhibitory neuron, respectively. There are eight kinds of combinations for M10 and M12 (i.e., EEE, EEI, EIE, IEE, IIE, IEI, EII, and III), which are listed in Table I. Due to the structure symmetry of M7 and M13, only four kinds of combinations are formed (i.e., EEE, EEI, IIE, and III).

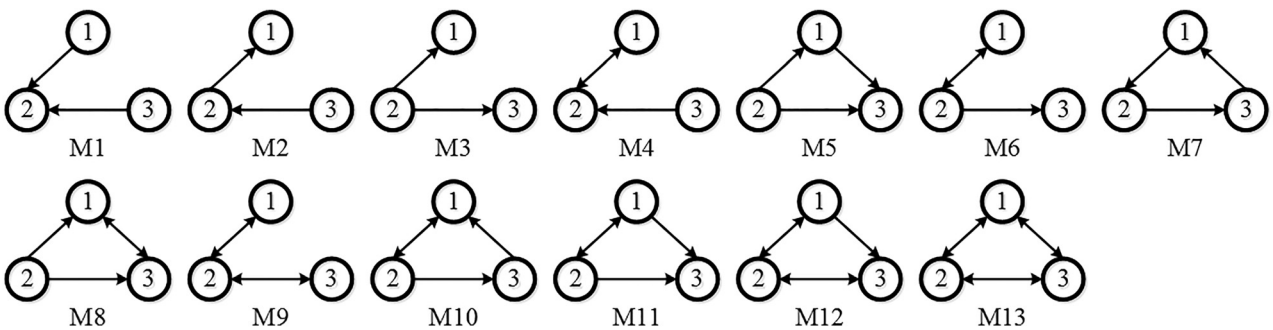

FIG. 1. List of motifs representing the possible connectivity patterns of three neurons. The candidate motif is matched to the 13 motif classes (M1–M13), numbers in each motif refer to the label of neurons.

TABLE I. Eight kinds of combinations of M10, here E and I are used to represent excitatory and inhibitory neurons, respectively.

Type	Neuron 1	Neuron 2	Neuron 3
T1-M10	E	E	E
T2-M10	E	E	I
T3-M10	E	I	E
T4-M10	I	E	E
T5-M10	I	I	E
T6-M10	I	E	I
T7-M10	E	I	I
T8-M10	I	I	I

B. Neuron model

Neurons are modeled by the Izhikevich equation,[50] which is described as follows:

$$\begin{aligned}\frac{dV_i}{dt} &= 0.04V_i^2 + 5V_i + 140 - u_i + I_i + I_{syn}^i,\\ \frac{du_i}{dt} &= a(bV_i - u_i),\end{aligned} \tag{1}$$

with the auxiliary after-spike resetting

$$\text{if } V_i \geq 30\,\text{mV}, \text{ then } \begin{cases} V_i \leftarrow c \\ u_i \leftarrow u_i + d, \end{cases} \tag{2}$$

where $i = 1, 2, 3$ index the neurons, V_i represents the membrane potential of the i-th neuron, and u_i is the corresponding membrane recovery variable. I_i is the injected dc-current, I_{syn}^i represents the synaptic input current. a, b, c, and d are the four adjustable parameters. According to Ref. 50, we use the regular spiking (RS) neuron ($a = 0.02, b = 0.2, c = -65, d = 8$) to model the excitatory neuron and the fast spiking (FS) neuron ($a = 0.1, b = 0.2, c = -65, d = 2$) to model the inhibitory neuron. I_i is set to be 10 for both the RS and FS neurons to make them fire regularly.[50]

C. Synapse model

For the chemical coupling considered in this work, the synaptic current projected into neuron i is the linear sum of all incoming synapses $I_{syn}^i = \sum_j I_{syn}^{ij}$ and the individual synaptic current I_{syn}^{ij} is

$$I_{syn}^{ij} = g_{ij} s_j (V_i - E_{syn}), \tag{3}$$

here g_{ij} is the maximal conductance of the synapse, unless stated otherwise, we assume that $g_{ij} = g$, that is to say, the coupling strength is identical for all connections. The reversal potential is set to be $E_{syn} = 0$ for excitatory synapse and $E_{syn} = -80$ for inhibitory synapse. The synaptic variable s_j is modeled using the fast threshold modulation (FTM) model proposed by Somers and Kopell in 1993 (Ref. 51)

$$s_j = \frac{1}{1 + \exp\left(-\lambda\left(V_j - \theta\right)\right)}, \tag{4}$$

when the presynaptic neuron voltage V_j is above the threshold θ, the postsynaptic neuron receives the synaptic current. Hereafter, parameters are set to be $\lambda = 0.15, \theta = 0$. The evolution of two mutually coupled RS and FS neuron and their corresponding synaptic variable is shown in Fig. 2. Note that neurons are coupled only when its presynaptic neuron is active, which conforms to the concept of chemical synapse. We wish to emphasize that the inter-node communication is instantaneous; hence, our network cannot account for the phenomenon related to synaptic transmission delay, because for small networks the transmission delays are negligible.[44–52]

D. Observability and controllability index of nonlinear systems

Nonlinear observability is tied to the measurement (output) function and its higher order Lie derivative with respect to the nonlinear system equations. For an affine nonlinear system

$$\begin{aligned}\dot{\mathbf{x}} &= \mathbf{f}(\mathbf{x}) + \mathbf{g}(\mathbf{x})\mathbf{u},\\ y &= h(\mathbf{x}),\end{aligned} \tag{5}$$

where $\mathbf{f} : R^n \to R^n, \mathbf{g} : R^n \to R^m, h : R^n \to R^1$, n and m represent the dimension of the state variable $\mathbf{x} = (x_1 \cdots x_n)^T$

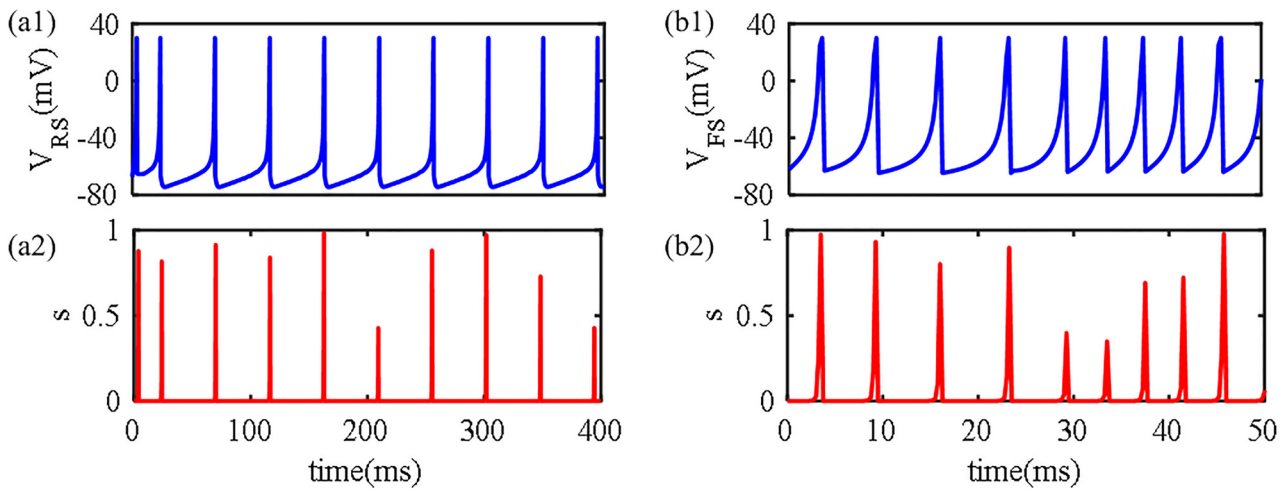

FIG. 2. Dynamics of two mutually coupled RS and FS neuron. (a1) and (b1) are the time evolution of the membrane potential of RS and FS neuron, respectively. (a2) and (b2) are the corresponding synaptic variable.

and the external input variable $\mathbf{u} = (u_1 \cdots u_m)^T$, $(\bullet)^T$ indicates the transpose. The output y represents the measured (observed) variable of the system. The observability problem here is to determine whether it is possible to estimate $\mathbf{x}$ from y. Usually it is analyzed without considering the external input, that is $\mathbf{g}(\mathbf{x})\mathbf{u} = 0$.

Differentiating $h(\mathbf{x})$ yields

$$\dot{y}(t) = \frac{d}{dt}h(\mathbf{x}) = \frac{\partial h}{\partial \mathbf{x}}\dot{\mathbf{x}} = \frac{\partial h}{\partial \mathbf{x}}\mathbf{f}(\mathbf{x}) = L_{\mathbf{f}}h(\mathbf{x}), \tag{6}$$

where $L_{\mathbf{f}}h(\mathbf{x})$ is the Lie derivative of h along the vector field $\mathbf{f}$. The j-th order Lie derivative is given by $L^j_{\mathbf{f}}h(\mathbf{x}) = \frac{\partial L^{j-1}_{\mathbf{f}}h(\mathbf{x})}{\partial \mathbf{x}}\mathbf{f}(\mathbf{x})$, and $L^0_{\mathbf{f}}h(\mathbf{x}) = h(\mathbf{x})$. Then, the differential embedding map Φ is defined as the Lie derivatives $L^0_{\mathbf{f}}h(\mathbf{x}) \cdots L^{n-1}_{\mathbf{f}}h(\mathbf{x})$.

Definition 1. The observability matrix is obtained by taking the Jacobin matrix of Φ

$$O(\mathbf{x}) = \frac{\partial \Phi}{\partial \mathbf{x}} = \begin{bmatrix} \frac{\partial L^0_{\mathbf{f}}\mathrm{h}(\mathbf{x})}{\partial x_1} \frac{\partial L^0_{\mathbf{f}}\mathrm{h}(\mathbf{x})}{\partial x_2} \cdots \frac{\partial L^0_{\mathbf{f}}\mathrm{h}(\mathbf{x})}{\partial x_n} \\ \frac{\partial L^1_{\mathbf{f}}\mathrm{h}(\mathbf{x})}{\partial x_1} \frac{\partial L^1_{\mathbf{f}}\mathrm{h}(\mathbf{x})}{\partial x_2} \cdots \frac{\partial L^1_{\mathbf{f}}\mathrm{h}(\mathbf{x})}{\partial x_n} \\ \vdots \\ \frac{\partial L^{n-1}_{\mathbf{f}}\mathrm{h}(\mathbf{x})}{\partial x_1} \frac{\partial L^{n-1}_{\mathbf{f}}\mathrm{h}(\mathbf{x})}{\partial x_2} \cdots \frac{\partial L^{n-1}_{\mathbf{f}}\mathrm{h}(\mathbf{x})}{\partial x_n} \end{bmatrix}. \tag{7}$$

Nonlinear controllability is tied to the input function and its higher order Lie bracket with respect to the system equation. Considering the two vector fields $\mathbf{f}(\mathbf{x})$ and $\mathbf{g}(\mathbf{x})$ in Eq. (5), the Lie bracket generates a new vector field

$$\begin{aligned} \left(ad^1_{\mathbf{f}}, \mathbf{g}\right) &= [\mathbf{f}, \mathbf{g}] = \frac{\partial \mathbf{g}}{\partial \mathbf{x}}\mathbf{f} - \frac{\partial \mathbf{f}}{\partial \mathbf{x}}\mathbf{g}, \\ \left(ad^2_{\mathbf{f}}, \mathbf{g}\right) &= [\mathbf{f}, [\mathbf{f}, \mathbf{g}]], \\ &\cdots \\ \left(ad^{n-1}_{\mathbf{f}}, \mathbf{g}\right) &= \left[\mathbf{f}, \left(ad^{n-2}_{\mathbf{f}}, \mathbf{g}\right)\right]. \end{aligned} \tag{8}$$

Definition 2. The nonlinear controllability matrix is defined as

$$C = \left[\mathbf{g}, \left(ad^1_{\mathbf{f}}, \mathbf{g}\right), \ldots \left(ad^{n-1}_{\mathbf{f}}, \mathbf{g}\right)\right]. \tag{9}$$

The system is called controllable if the determinant of the controllability matrix never vanishes, that is

$$\det(C(\mathbf{x})) \neq 0. \tag{10}$$

The definition of observable is similar to controllable, with C substituted by O. This definition is "yes" or "no" measures, namely, the system is either controllable or not. Thus, the controllability (observability) index is introduced by researchers, which is a continuous function of system parameters and can be used to evaluate how far the system is from uncontrollable (unobservable).[49]

Definition 3. The controllability index is quantified to represent the degree of controllability, defined as

$$\delta(\mathbf{x}) = \left.\frac{|\lambda_{\min}(C^TC)|}{|\lambda_{\max}(C^TC)|}\right|_{\mathbf{x}(t)}, \tag{11}$$

where $\lambda_{\min}(C^TC)$ and $\lambda_{\max}(C^TC)$ are the smallest and largest eigenvalues of matrix C^TC at point $\mathbf{x}(t)$, and $(\bullet)^T$ also indicates the transpose. It should be noticed that $0 < \delta(\mathbf{x}) < 1$, the lower bound is attained when the system is uncontrollable at point $\mathbf{x}(t)$, while the upper bound indicates full controllability. The definition of controllability index is a type of condition number of matrix C^TC. From the definition $\delta(\mathbf{x})$ is a local measure, which depends on the point $\mathbf{x}(t)$ of the system. In this paper, we use the average value of each time point to represent the controllability of the node[53]

$$\bar{\delta} = \frac{1}{T}\sum_{t=0}^{T}\delta(\mathbf{x}(t)). \tag{12}$$

Here, T is the whole time span of variable $\mathbf{x}$. The definition of the observability index is similar to the controllability index, with C substituted by O.

E. Observability and controllability of the 3-Izhikevich neuron motifs

Assuming the control signal is added to neuron 1, then the process of calculating the controllability (observability) matrix is introduced here as an illustration. First, we transform the system into the form of Eq. (5). The state vector is set to be $\mathbf{x} = (V_1u_1V_2u_2V_3u_3)^T$, such that we get the transformed system equations as follows:

$$\begin{aligned} \dot{\mathbf{x}} &= [\dot{V}_1\dot{u}_1\dot{V}_2\dot{u}_2\dot{V}_3\dot{u}_3]^T = \mathbf{f}(\mathbf{x}) + \mathbf{g}(\mathbf{x})\mathbf{u}, \\ \mathbf{f}(\mathbf{x}) &= \begin{bmatrix} 0.04V_1^2 + 5V_1 + 140 - u_1 + I_1 + I^1_{syn} \\ a_1(b_1V_1 - u_1) \\ 0.04V_2^2 + 5V_2 + 140 - u_2 + I_2 + I^2_{syn} \\ a_2(b_2V_2 - u_2) \\ 0.04V_3^2 + 5V_3 + 140 - u_3 + I_3 + I^3_{syn} \\ a_3(b_3V_3 - u_3) \end{bmatrix}, \\ \mathbf{g}(\mathbf{x}) &= [1\ 0\ 0\ 0\ 0\ 0]^T. \end{aligned} \tag{13}$$

Then, the controllability and observability matrix can be obtained through Eqs. (7) and (9), respectively.

F. Simulation protocol

The simulated data of state variables of the 3-Izhikevich neuron network are obtained in MATLAB R2014b by solving the differential equations using the Euler's method, with a time step of 0.25 ms. The initial states of excitatory and inhibitory neuron are set to be $(-70, -70 \cdot b)$ and $(-64, -64 \cdot b)$, respectively. The symbolic computation of the controllability (observability) matrix is realized in Mathematica 10.0. Then, the membrane potential and membrane recovery variable dataset of neurons obtained in MATLAB is imported to Mathematica to calculate the observability index of each time point. Finally, the mean controllability (observability) index is obtained by averaging the indexes of all time points.

III. CONTROLLABILITY (OBSERVABILITY) ANALYSIS OF THE 3-IZHIKEVICH NEURON MOTIFS

Since we are interested in exploring the controllability (observability) of networks motifs with different neuron and synaptic dynamics, we first confirm that these dynamics do affect the control (observe) ability of the network nodes. Then, we analyze how various dynamics behave differently in shaping the node controllability (observability).

A. Controllability (observability) analysis of M7 and M13 with different neuron types

Due to the structure symmetry of M7 and M13, only four types of combinations (EEE, EEI, IIE, III) are constructed. The synaptic conductance is chosen to be $g = 0.2$ for both excitatory and inhibitory coupling. Then, the controllability (observability) index of each node is calculated using Eq. (12). As shown in Fig. 3, for M7, all nodes are controllable (observable). The indexes of these three nodes are the same when node properties are identical (EEE, III) because of the cyclic symmetric structure. However, when the node properties are different the indexes are different. What is more, the most controllable (observable) node varies too. For M13, when the properties of each node are the same, all nodes in the network are not controllable (observable) due to the rotational symmetry. However, the uncontrollable (unobservable) nodes in the homogeneous networks (e.g., EEE and III) will become controllable (observable) if the symmetry is broken by introducing heterogeneous node (e.g., IEE and IIE). Therefore, it is necessary to take the node dynamics into consideration when selecting the best driver (sensor) node to modulate (observe) the whole network activity.

B. Inhibitory motifs are more controllable (observable) than excitatory motifs

In this section, we compare the controllability (observability) of excitatory and inhibitory motifs, and the coupling strength is also set to be $g = 0.2$ for both excitatory and inhibitory synapses. Fig. 4 presents the indexes of each node measured from M10 and M12. It is noticed that for both motifs, nodes in the inhibitory construction (i.e., T8-III) are more controllable (observable) than the excitatory one (i.e., T1-EEE). We calculate the evolution of the membrane potential, the controllability index, and the observability index of each node for T1-M10 and T8-M10 to investigate the difference between T8-III and T1-EEE. As shown in Fig. 5, neurons in the inhibitory network fire faster than those in the excitatory network, and the maximum values of these two indexes are corresponding to the peak values of the membrane potential. Thus, neurons in the inhibitory network have more maxima, besides the maximum value of each node in T8-M10 is larger than the corresponding node in T1-M10, so the mean index is certainly higher.

C. Controllability (observability) analysis of 8-kind M10 with different coupling strengths

In this section, we mainly explore the effects of synaptic coupling strength on the controllability (observability) of the motifs. The synaptic conductance is increased from 0.1 to 1 with an increment of 0.1 to simulate the variation of coupling strength. The mean index of all three nodes is used to

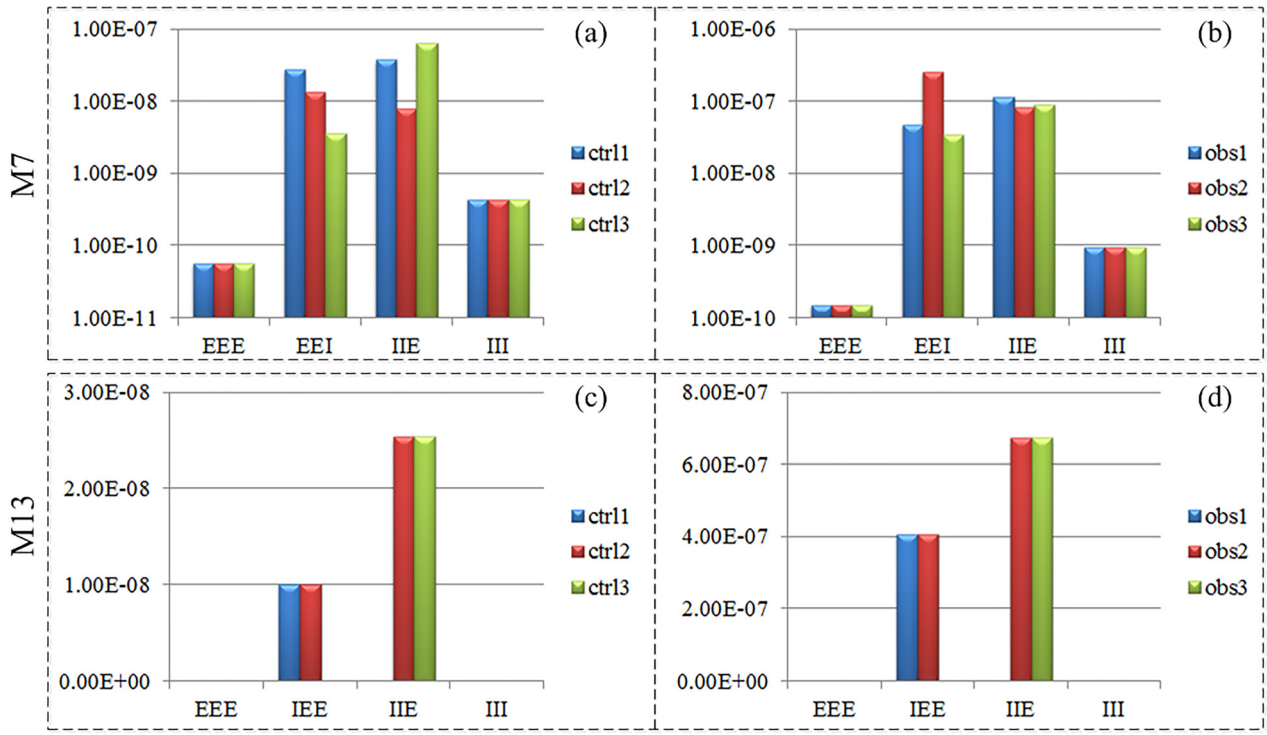

FIG. 3. (a) and (b) Controllability and observability index of each node in M7 with four kinds of network combinations. (c) and (d) Controllability and observability index of each node in M13 with four kinds of network combinations. "ctr1" represents the controllability index of node 1, and "obs1" represents the observability index of node 1. "E" is the excitatory RS neuron, and "I" is the inhibitory FS neuron.

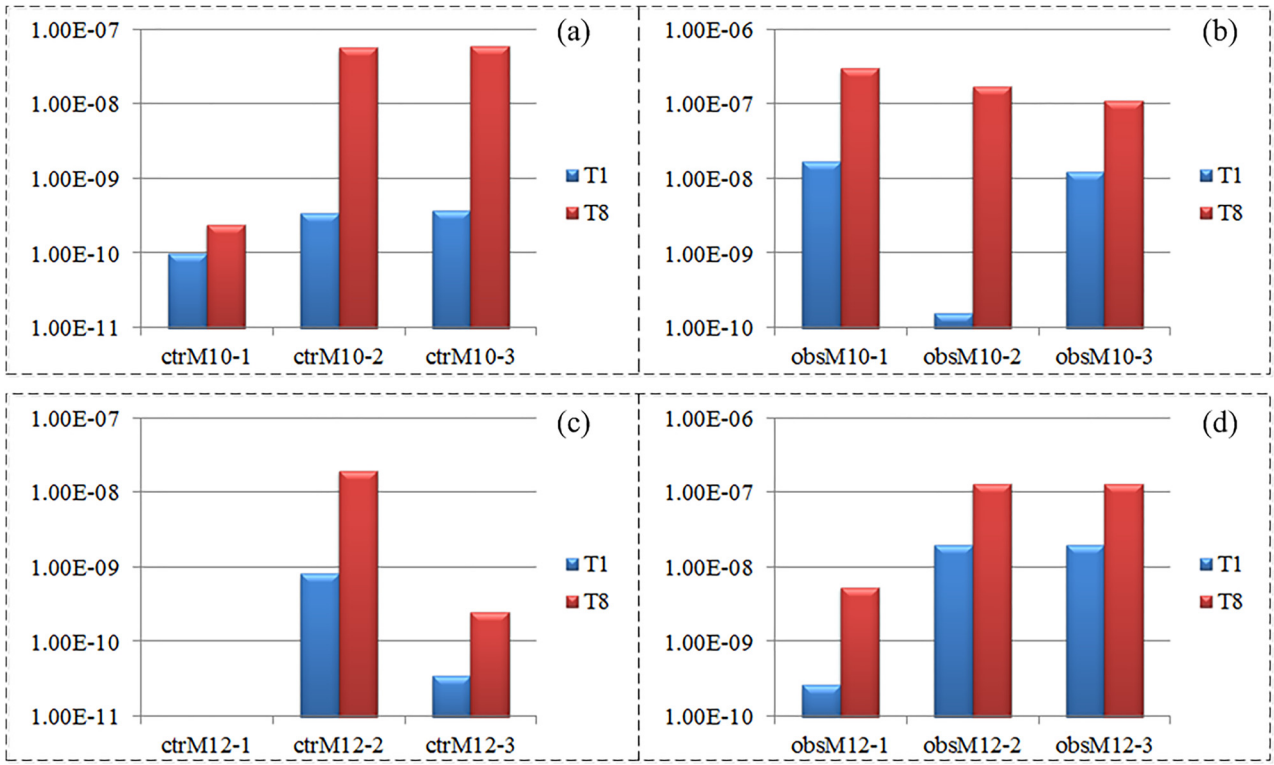

FIG. 4. (a) and (b) Controllability and observability index of each node in T1 (EEE) and T8 (III) type M10. (c) and (d) Controllability and observability index of each node in T1 (EEE) and T8 (III) type M12. "ctrM10-1" represents the controllability index of node 1 in M10, and "obsM10-1" represents the observability index of node 1 in M10.

quantify the network controllability (observability). As shown in Fig. 6, when the coupling strength $g = 0.1$, the indexes are the smallest. The indexes show an increasing trend for all eight kinds of networks with the increment of coupling strength, when the coupling strength $g > 0.7$, the increasing trend becomes slower.

IV. APPLY THE CONTROLLABILITY ANALYSIS RESULTS IN MOTIFS TO DESYNCHRONIZATION CONTROL OF MODULAR NETWORK

The above simulations demonstrate that the controllability and observability of different nodes in the same network are different. Therefore, the control energy needed to modulate the network dynamics towards the desired state may vary depending on which node is selected as the driver node. In this section, we generalize the controllability analysis to the desynchronization control of modular motif network in order to verify the selection method of the best driver node. The closed-loop goal driven control method is introduced to calculate the external current applied to the selected node.

Studies about the connectivity between regions of the cerebral cortex revealed that cortex networks were modular networks and composed of certain sub-networks with different internal and external connectivity.[54,55] Here, these sub-networks are chosen as the T1-M10 motifs (Fig. 7). The

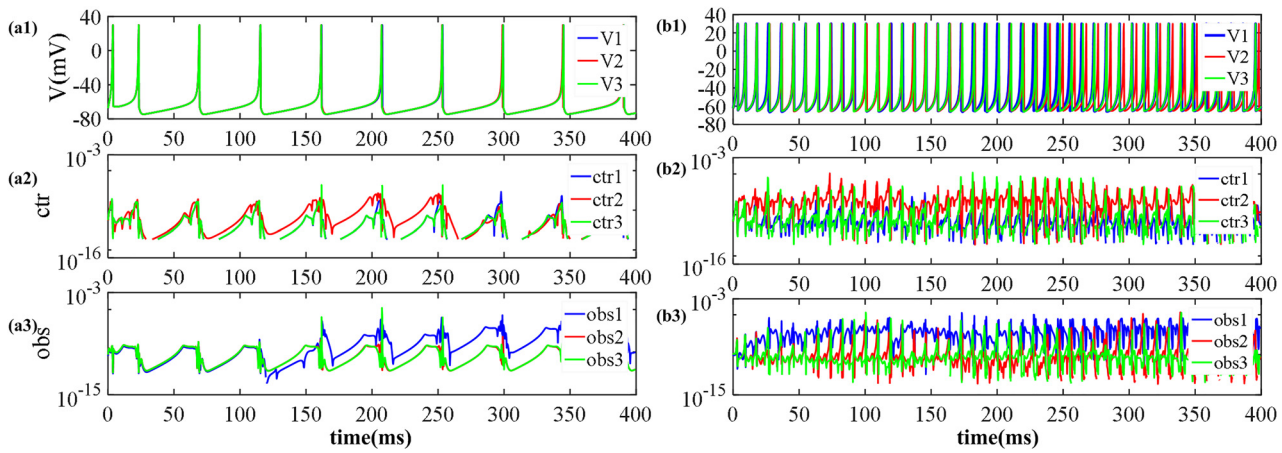

FIG. 5. Time evolution of the membrane potential (a1) and (b1), the controllability index (a2) and (b2) and the observability index (a3) and (b1) of each node in T1-M10 and T8-M10, respectively.

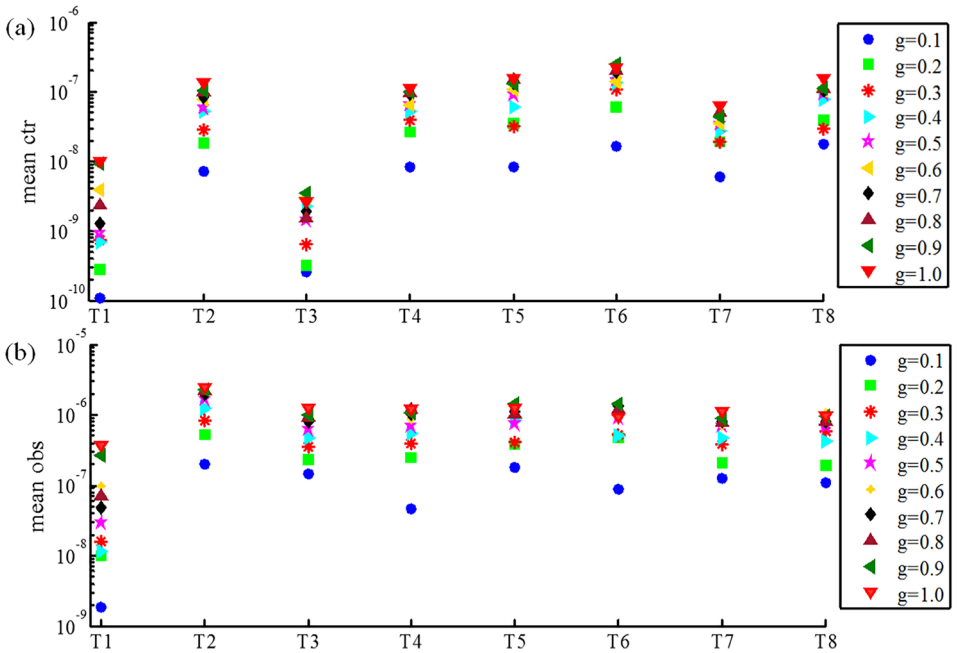

FIG. 6. The mean controllability (observability) index of the three nodes in M10 with eight kinds of constructions (T1–T8) under different coupling strengths ($g = 0.1$ to $g = 1.0$).

internal coupling strength within the motif is $g = 0.4$, and the external coupling strength among motifs is $g = 0.1$. Since motifs have more than one node and edge, lots of possibilities exist for motifs being connected into modular networks, the exchange of information among motifs is achieved through node 2 in this study.

The control goal is to desynchronize the network dynamics, which means tracking the desired asynchronous dynamics through the modulation of control signal. The mean membrane potential of 27 neurons is used to indicate the network synchronization situation.[56] The desired membrane potential $mean\_V_d(t)$ is obtained by setting the initial states of 27 neurons to random values when calculating the differential equations. The synchronized and desynchronized mean membrane potential $mean\_V(t)$ and $mean\_V_d(t)$ are shown in Figs. 8(a) and 8(b), respectively. The simple P-type iterative learning control (ILC) algorithm with the concept of forgetting factor[57,58] is used to calculate the control signal, which can be described as follows:

$$ctr_{k+1}(t) = \alpha ctr_k(t) + (1-\alpha)ctr_{k-1}(t) + Ke_k(t), \qquad (14)$$

where K is the proportional gain, and $0 < \alpha < 1$ is the forgetting factor. ctr_{k+1}, ctr_k, and ctr_{k-1} are the control signals of the $(k+1)$-th, k-th and $(k-1)$-th iterative process, respectively. $e_k(t) = mean\_V_d(t) - mean\_V(t)$ is the tracking error. The block diagram of the closed-loop ILC system is presented in Fig. 8(c), where the goal is to calculate an optimal control signal $ctr(t)$ by evaluating the track error $e_k(t)$.

In order to select the appropriate controller parameters and further assess the performance of the controller, two indexes are defined:

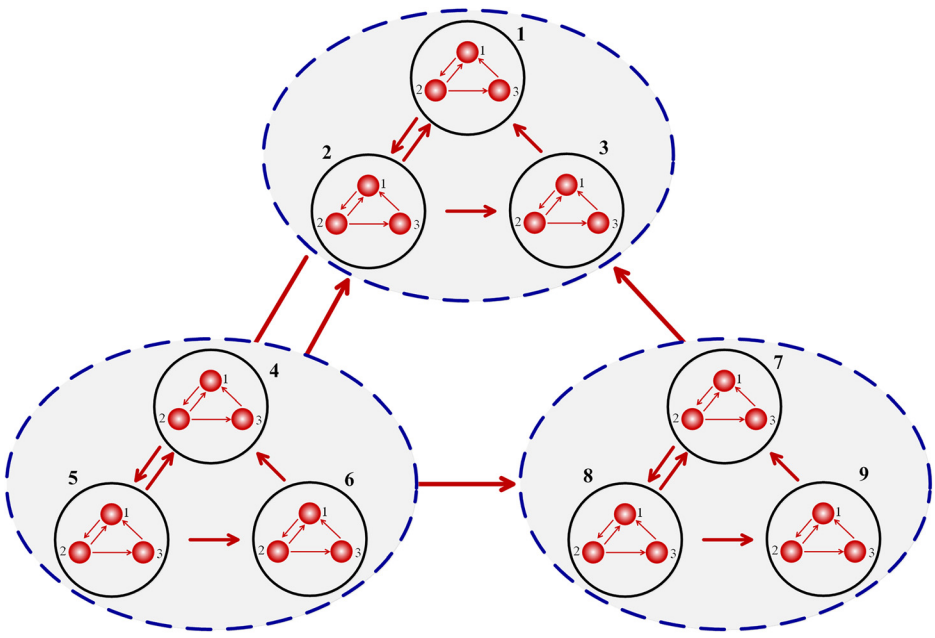

FIG. 7. The connection diagram of the modular network. Numbers 1–9 in the dotted blue circle represent the label of each motif. Numbers 1–3 in the black solid circle represent the number of each neuron in the motif.

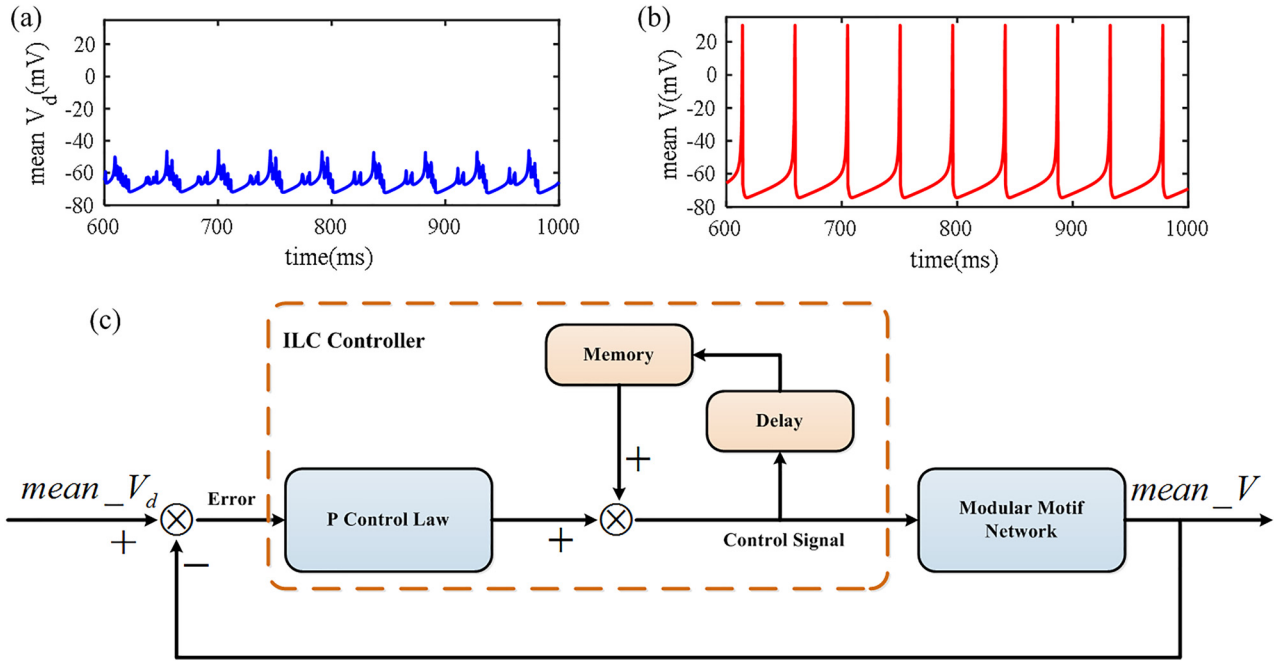

FIG. 8. (a) The desired mean membrane potential under asynchronous network state. (b) The controlled mean membrane potential under synchronous network state. (c) The block diagram of the closed-loop P-type ILC system.

A. Energy expenditure

The magnitude of the control signal is assumed to be proportional to the rate of fuel consumption.[8] The associated control effort in the root-mean-square (RMS) form is defined as follows:

$$u_{RMS} = \sqrt{\frac{1}{T}\int_T ctr_k{}^2 dt}, \tag{15}$$

where T is the time span of the whole simulation, and ctr_k is the stimulation signal added to the node of the k-th iterative process.

B. Neuronal synchrony measure

As the control aim is to desynchronize the network dynamics, the neuronal synchrony index proposed in Ref. 59 is used to quantify the desynchronization performance. $V_i(t)$ is the membrane potential of the i-th neuron. The mean membrane potential of the 27 neurons in the modular motif network is defined by

$$mean\_V = \frac{1}{27}\sum_{i=1}^{27} V_i(t). \tag{16}$$

The variance of the time fluctuations of $mean\_V$ is

$$\sigma^2_{mean\_V} = \frac{1}{T}\int_0^T mean\_V^2(t)dt - \left(\frac{1}{T}\int_0^T mean\_V(t)dt\right)^2. \tag{17}$$

Also, the variance of the single cell membrane potential is

$$\sigma^2_{V_i} = \frac{1}{T}\int_0^T V_i{}^2(t)dt - \left(\frac{1}{T}\int_0^T V_i(t)dt\right)^2. \tag{18}$$

The synchrony measure χ is defined as follows:

$$\chi = \frac{\sigma^2_{mean\_V}}{\frac{1}{27}\sum_{i=1}^{27}\sigma^2_{V_i}}, \tag{19}$$

where $\chi \in [0,1]$, in particular, the system is fully synchronized if $\chi = 1$ and in the asynchronous state $\chi = 0$.

In order to quantify the controllability of each node, the control signal is added to only one node at a time, which was proved to be an effective way of desynchronizing network dynamics.[60,61] So, comparisons are made among 27 trials. The appropriate control parameters for each node are obtained when $\chi \in [0.031, 0.032]$ is first satisfied, and then choose the parameters corresponding to the minimum u_{RMS}. The range of parameters is restricted to $\alpha \in [0,1]$, $K \in [3,5]$ via trial-and-error. The best control parameters are obtained through traversing between the above region with a step of 0.01 and 0.05, which are listed in Table II. The total iterative time is 80 for every trial.

The corresponding energy expenditure of the stimulation signal is presented in Fig. 9. The lowest energy consumption is achieved when node "52" is chosen as the controlled node, thus we can deduce that node "52" is the best driver node with highest controllability. In above controllability analysis of single T1-M10 motif, the most controllable node is node 2. So when the control signal is added to the nodes of motifs 4, 5, 6, the energy expenditure is lower than motifs 1, 2, 3 and 7, 8, 9, because motifs 4, 5, and 6 represent the node 2 of the large modular network. Besides, motif 5 is node 2 among motifs 4, 5, and 6, and

TABLE II. The best control parameters for different driver nodes (e.g., "11" represents the first node of motif 1).

	11	**12**	**13**	**21**	**22**	**23**	**31**	**32**	**33**	**41**	**42**	**43**	**51**	**52**
K	5	4.3	4.85	4.2	4.85	4.55	4.65	4.1	4.85	4.3	4.8	4.1	4.55	4.05
α	0.5	0	0.1	0.1	0.1	0	0.4	0	0.2	0.2	0.4	0	0.2	0.2
	53	**61**	**62**	**63**	**71**	**72**	**73**	**81**	**82**	**83**	**91**	**92**	**92**	
K	5	3.45	4.65	4.5	4.1	3.9	4.15	4.85	4.85	5	3.35	4.9	4.35	
α	0.5	0	0.2	0	0.2	0	0.1	0.4	0.4	0.2	0	0.2	0.1	

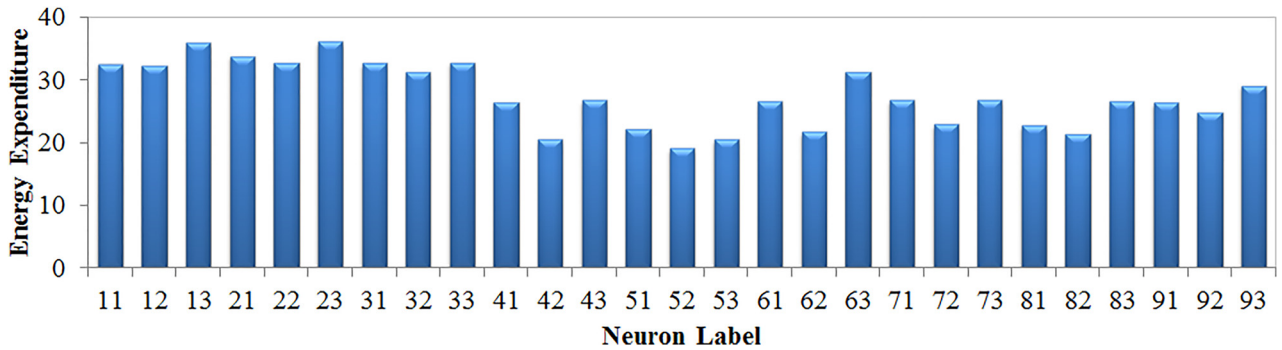

FIG. 9. Energy expenditure of the stimulation input for different driver nodes. The horizontal axis is the label of selected driver node, and the vertical axis is the corresponding value of energy expenditure.

then node "52" is the most controllable node in motif 5. Therefore, results obtained in this extended modular network are in line with the controllability analysis in small motifs.

V. CONCLUSION

The function of brain networks is closely tied to the temporal characteristic of neurons, the synaptic coupling types as well as the network topological structure. Understanding the role of each element will help modulate the brain activity towards a desired state in an optimal manner. The beforehand controllability (observability) analysis of corresponding brain networks is deemed to be necessary for better selecting the control signal. Previous studies have broadly reported the crucial role of network topology in determining the appropriate driver or sensor nodes. Here, we particularly emphasize the impacts of intrinsic node state (excitatory and inhibitory) and the synaptic coupling strength. Therefore, motifs consisting of excitatory RS neurons and inhibitory FS neurons are first investigated. The nonlinear controllability (observability) analytical method from the differential geometry is used to calculate the controllability (observability) of certain node in the motifs.

Through the numerical simulations, we first demonstrate that the properties of single node and the synaptic coupling strength do affect the controllability (observability) of the node. The inhibitory network is more controllable (observable) than the excitatory one with the same topological structure. Furthermore, controllability analysis results obtained from the excitatory motif are validated by the desynchronization control of the modular motif network. There is still a long way to go to before extending all controllability (observability) analysis in motifs to large network control, which is our future research direction.

The brain is a modular network. Spiking activity can propagate from one module to another with high precision.[62] However, the existence of noise could disrupt millisecond precision during the transmission. Feed-forward networks are extensively used to investigate the propagation of neural activities.[31,63] Motifs are constituent elements of feed-forward networks, determining the signal propagation. In general, the robustness of signal propagation is always better for networks with higher controllability or observability. Because the spike patterns of neurons are easier to be controlled or observed with high precision from other nodes. Therefore, it is expected that high controllability or observability may promote the propagation process.

ACKNOWLEDGMENTS

This work was supported by the National Natural Science Foundation of China (Grant Nos. 61374182, 61471265, and 61302002), the China Scholarship Council's Study Abroad Project (No. 201606250142), and the Tangshan Technology Research and Development Program (Grant No. 14130223B).

[1]A. B. Schwartz, X. T. Cui, D. J. Weber, and D. W. Moran, Neuron **52**, 205–220 (2006).
[2]J. A. Bauer, K. M. Lambert, and J. A. White, IEEE Trans. Biomed. Eng. **61**, 1448–1456 (2014).
[3]D. Linaro, J. Couto, and M. Giugliano, J. Neurosci. Methods **230**, 5–19 (2014).
[4]R. Carron, A. Chaillet, A. Filipchuk, W. Pasillas-Lépine, and C. Hammond, Front. Syst. Neurosci. **7**, 00112 (2013).
[5]A. Berenyi, M. Belluscio, D. Mao, and G. Buzsaki, Science **337**, 735–737 (2012).
[6]S. J. Schiff, *Neutral Control Engineering: The Emerging Intersection Between Control Theory and Neuroscience* (The MIT Press, London, 2012).

[7]A. J. Whalen, S. N. Brennan, T. D. Sauer, and S. J. Schiff, Phys. Rev. X **5**, 011005 (2015).
[8]Y. Y. Liu and A. L. Barabási, Rev. Mod. Phys. **88**, 035006 (2016).
[9]Y. Y. Liu, J. J. Slotine, and A. L. Barabási, Nature **473**, 167–173 (2011).
[10]Z. Z. Yuan, C. Zhao, Z. R. Di, W. X. Wang, and Y. C. Lai, Nat. Commun. **4**, 167–173 (2013).
[11]J. Li, L. Dueñas-Osorio, C. K. Chen, B. Berryhill, and A. Yazdani, Physica A **453**, 84–98 (2016).
[12]Q. Y. Miao, Y. Tang, J. Kurths, J. A. Fang, and W. K. Wong, Chaos **23**, 033114 (2013).
[13]B. Barzel, Y. Y. Liu, and A. L. Barabási, Nat. Commun. **6**, 7186 (2015).
[14]X. F. Li, Z. M. Lu, and H. Li, Int. J. Mod. Phys. C **26**, 1550028 (2015).
[15]C. Zhao, W. X. Wang, Y. Y. Liu, and J. J. Slotine, Sci. Rep. **5**, 8422 (2015).
[16]J. C. Nacher and T. Akutsu, Sci. Rep. **3**, 1647 (2013).
[17]T. Jia and A. L. Barabási, Sci. Rep. **3**, 2354 (2013).
[18]J. H. Zhao, H. J. Zhou, and Y. Y. Liu, Nat. Commun. **4**, 2412 (2013).
[19]C. L. Pu, W. J. Pei, and A. Michaelson, Physica A **391**, 4420–4425 (2012).
[20]Y. Y. Liu, J. J. Slotine, and A. L. Barabasi, Proc. Natl. Acad. Sci. U. S. A. **110**, 2460–2465 (2013).
[21]T. J. Lewis and J. Rinzel, J. Comput. Neurosci. **14**, 283–309 (2003).
[22]V. S. Afraimovich and L. A. Bunimovich, Nonlinearity **20**, 1761–1771 (2007).
[23]H. T. Yu, J. Wang, C. Liu, B. Deng, and X. L. Wei, Physica A **405**, 25–34 (2014).
[24]R. Uzun, M. Ozer, and M. Perc, Europhys. Lett. **105**, 60002 (2014).
[25]X. J. Sun, J. Z. Lei, M. Perc, J. Kurths, and G. R. Chen, Chaos **21**, 016110 (2011).
[26]Q. Y. Wang, M. Perc, Z. S. Duan, and G. R. Chen, Chaos **19**, 023112 (2009).
[27]M. Perc, Chaos, Soliton Fractals **31**, 280–291 (2007).
[28]J. M. Coron, *Control and Nonlinearity* (American Mathematical Society, 2007).
[29]C. Luo, X. Y. Wang, and H. Liu, Chaos **24**, 033108 (2014).
[30]C. Letellier, J. Maquet, L. Le Sceller, G. Gouesbet, and L. A. Aguirre, J. Phys. A: Math. Gen. **31**, 7913–7927(1998).
[31]R. X. Han, J. Wang, H. T. Yu, B. Deng, X. L. Wei, Y. M. Qin, and H. X. Wang, Chaos **25**, 043108 (2015).
[32]S. Jalil, I. Belykh, and A. Shilnikov, Phys. Rev. E **85**, 036214 (2012).
[33]R. A. Stefanescu and V. K. Jirsa, PLoS Comput. Biol. **4**, e1000219 (2008).
[34]H. H. Zhang, Q. Y. Wang, M. Perc, and G. R. Chen, Commun. Nonlinear Sci. Numer. Simul. **18**, 601–615 (2013).
[35]D. Q. Guo, M. M. Chen, M. Perc, S. D. Wu, C. Xia, Y. S. Zhang, P. Xu, Y. Xia, and D. Z. Yao, Europhys. Lett. **114**, 30001 (2016).
[36]D. Q. Guo, S. D. Wu, M. M. Chen, M. Perc, Y. S. Zhang, J. L. Ma, Y. Cui, P. Xu, Y. Xia, and D. Z. Yao, Sci. Rep. **6**, 26096 (2016).
[37]B. Haider, A. Duque, A. R. Hasenstaub, and D. A. McCormick, J. Neurosci. **26**, 4535–4545 (2006).
[38]W. W. Lytton, Nat. Rev. Neurosci. **9**, 626–637 (2008).
[39]A. Kumar, S. Cardanobile, S. Rotter, and A. Aertsen, Front. Syst. Neurosci. **5**, 00086 (2011).
[40]R. Milo, Science **298**, 824–827 (2002).
[41]O. Sporns and R. Kotter, PLoS Biol. **2**, e369 (2004).
[42]S. Song, P. J. Sjostrom, M. Reigl, S. Nelson, and D. B. Chklovskii, PLoS Biol. **3**, e68 (2005).
[43]R. J. Prill, P. A. Iglesias, and A. Levchenko, PLoS Biol. **3**, e343 (2005).
[44]D. Q. Guo and C. G. Li, Phys. Rev. E **79**, 051921 (2009).
[45]L. L. Gollo, C. Mirasso, O. Sporns, and M. Breakspear, PLoS Comput. Biol. **10**, e1003548 (2014).
[46]O. D'Huys, R. Vicente, T. Erneux, J. Danckaert, and I. Fischer, Chaos **18**, 037116 (2008).
[47]E. M. Izhikevich, *Dynamical Systems in Neuroscience: The Geometry of Excitability and Bursting* (The MIT Press, London, 2005).
[48]A. Sedoglavic, J. Symbolic Comput. **33**, 735–755 (2002).
[49]B. Friedland, J. Dyn. Syst. - Trans. ASME **97**, 444–445 (1975).
[50]E. M. Izhikevich, IEEE Trans. Neural Networks **14**, 1569–1572 (2003).
[51]D. Somers and N. Kopell, Biol. Cybern. **68**, 393–407 (1993).
[52]B. Ibarz, H. Cao, and M. Sanjuán, Phys. Rev. E **77**, 051918 (2008).
[53]L. A. Aguirre, IEEE Trans. Educ. **38**, 33–39 (1995).
[54]C. C. Hilgetag, G. A. P. C. Burns, M. A. O'Neill, J. W. Scannell, and M. P. Young, Philos. Trans. R. Soc. B **355**, 91–110 (2000).
[55]C. C. Hilgetag and M. Kaiser, Neuroinformatics **2**, 353–360 (2004).
[56]O. Popovych and P. A. Tass, Front. Neurol. **5**, 268 (2014).
[57]H. S. Ahn, Y. Chen, and K. L. Moore, IEEE Trans. Syst., Man, Cybern., C **37**, 1099–1121 (2007).
[58]J. L. Chien and J. S. Liu, Int. J. Control **64**, 319–334 (1996).
[59]D. Golomb, Scholarpedia **2**, 1347 (2007).
[60]H. T. Yu, J. Wang, B. Deng, X. L. Wei, Y. K. Wong, W. L. Chan, K. M. Tsang, and Z. Q. Yu, Chaos **21**, 013127 (2011).
[61]A. Jabi and J. Moehlis, J. Neural Eng. **8**, 065008 (2011).
[62]A. Kumar, S. Rotter, and A. Aertsen, Nat. Rev. Neurosci. **11**, 615–627 (2010).
[63]S. Moldakarimov, M. Bazhenov, and T. J. Sejnowski, Proc. Natl. Acad. Sci. U. S. A. **112**, 2545–2550 (2015).